Thesis_plag_report_1.docx

by Mahima Helna

Submission date: 25-May-2026 05:00PM (UTC+0530)
Submission ID: 2969089646
File name: Thesis_plag_report_1.docx (5.32M)
Word count: 7352
Character count: 42738

ABSTRACT

In this work, neodymium (Nd^{3+})-substituted barium bismuth niobate ceramics, $BaBi_{2-x}Nd_xNb_2O_9$ (x = 0.00, 0.04, 0.06, 0.08, and 0.10), belonging to the Aurivillius family, were systematically investigated to examine the influence of Bi-site doping on the structural, dielectric, and energy-storage properties. All compositions were synthesized via the conventional solid-state route and sintered at 1050 °C. XRD analysis confirmed the formation of a single-phase orthorhombic Aurivillius structure, indicating successful incorporation of Nd^{3+} with minimal lattice distortion. SEM analysis revealed plate-like grains with a reduction in grain size upon doping. FTIR analysis confirmed the retention of characteristic NbO_6 vibrational bands, indicating preservation of the layered Aurivillius framework after Nd^{3+} substitution. Dielectric studies exhibited broad, frequency-dependent peaks, confirming relaxor behavior with the diffuseness parameter γ ranging from 1.45 to 1.75. DC conductivity decreased with increasing Nd content due to enhanced resistivity. Slim P–E loops with reduced remnant polarization favored energy-storage performance, with $BaBi_{1.94}Nd_{0.06}Nb_2O_9$ exhibiting an efficiency exceeding 90%. Raman and DRS analyses confirmed the preservation of the crystal structure and tunable band gaps, highlighting the strong potential of these ceramics for lead-free energy-storage applications.

CHAPTER-1

INTRODUCTION

1.1 BACKGROUND

Ferroelectric ceramics are materials that naturally develop an electric polarisation, which can be reversed by applying an external electric field [1]. Dipoles are aligned in certain directions in tiny domains. In ferroelectric ceramics, the electric polarisation is inherently present but can be altered by applying an electric field. Dipoles are oriented in specific directions in these ceramics. As a result, these features are widely used in sensors, actuators, capacitors, and memory devices. Due to their strong polarisation, ease of adjustment with an electric field, and ability to control their domain structure, these materials are often selected as host materials[2]. Additionally, they are multifunctional, showing electrical, optical, piezoelectric, and pyroelectric properties. Therefore, ferroelectric ceramics provide better energy storage, switchable polarisation for memory applications, and useful sensing properties for various electronic and thermal devices. Rare earth elements are often used as dopants in ferroelectric ceramics because they significantly improve the material's overall performance. Their addition helps introduce relaxor type behaviour, which leads to broader and more stable phase transitions[3]. Rare-earth doping also enhances dielectric properties, making the material more suitable for energy storage applications. These elements help stabilize ferroelectric polarisation, improve grain growth control, and allow better tuning of the microstructure. Another important benefit is the reduction of leakage current, which increases the efficiency and reliability of devices. In addition, rare-earth dopants improve the thermal stability of the material, making it more effective for high-temperature and high-performance applications[4].

Recently, lead-free materials have been getting more attention in the research world due to the various environmental and health issues caused by lead, and it has taken a diversion towards the Aurivillius compounds, which is the family of bismuth layered perovskite type oxides having the general formula $(Bi_2O_2)^{2+}(A_{n-1}B_nO3_{n+1})^{2-}$ [5, 6]. The A site cations are usually the large ions or the rare earth ions, which are ionically compatible with Bi^{3+} in the $(Bi_2O_2)^{2+}$ layers, whereas the B-site cations are smaller ions. The value of n indicates the number of perovskite layers sandwiched between Bi_2O_2 sheets. Here, we investigate barium bismuth niobate, generally abbreviated as BBN, where the value of n is 2, implying it has two perovskite-like layers between the $(Bi_2O_2)^{2+}$ sheets[7-9],. BBN is a relaxor ferroelectric having larger maximum polarisation and lesser remnant polarisation, and thus coming under the category of Bismuth Layered-Structured Ferroelectrics, abbreviated as BLSF [9], BLSFs are considered strong alternatives to lead-based ceramics because they are non-toxic and environmentally friendly. This makes them a better and safer option for modern applications. Lead-free BLSF materials have gained a lot of interest since they offer several useful properties, such as a relatively high dielectric constant, resistance to fatigue, high phase transition temperatures, good electromechanical anisotropy, and excellent stability over a wide temperature range [10-12]. Neodymium (Nd3+) is selected because of its limited published work, specifically Nd-doped BBN. Prior studies on Nd-doped $SrBi_2Nb_2O_9$ (SBN) and related Aurivillius-type compounds have shown enhanced ferroelectric, dielectric, and fatigue endurance because of a reduction in the generation of unwanted oxygen vacancies, which improves dielectric stability and optical properties due to its characteristic 4f-4f transitions in the near infrared region

(NIR)[13]. This provided a strong foundation for expecting similar or improved behaviour in Nd-doped BBN systems as well. Also, neodymium has an identical valence state to Bi3+ and ionic radius very close to BBN (Nd^{3+} ≈ 1.11 Å; Bi^{3+} ≈ 1.17 Å for 12 coordination number), which allows substitution without significant lattice distortion. This reduced distortion leads to better lattice symmetry and thermal stability.

This research explores the incorporation of Nd^{3+} (0.04, 0.06,0.08,0.10) into the BBN matrix to fine tune the structural, ferroelectric, and dielectric properties employing techniques such as X-ray diffraction, scanning electron microscopy, fourier transform infra-red spectroscopy, diffuse reflectance spectroscopy, Raman spectroscopy, polarisation electric field characterisation and dielectric spectroscopy to illuminate these effects. Barium bismuth niobate ($BaBi_2Nb_2O_9$) finds applications in ferroelectric memories [FeRAM], high-temperature piezoelectric sensors, dielectric capacitors, and energy-related devices due to its robust polarisation, thermal stability, and layered perovskite structure.

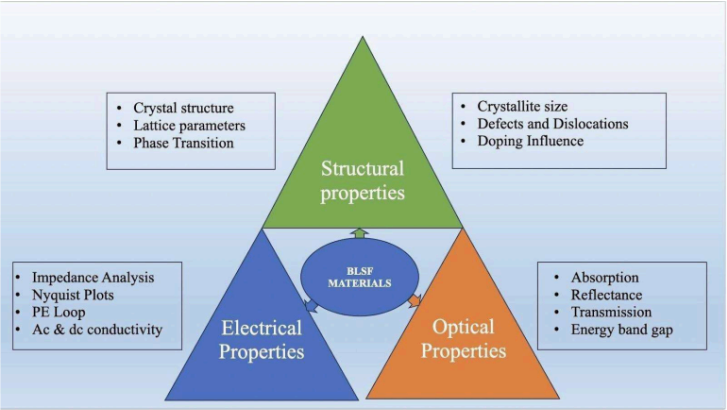

Fig 1.1

1.2 LITERATURE REVIEW 1

Temperature stability and improved energy storage efficiency of $BaBi_2Nb_2O_9$: Er^{3+}/Yb^{3+} relaxor ferroelectric ceramic under moderate electric fields.[9]

Ankita Banwal · Manoj Verma · Bharti Singh · Renuka Bokolia

Samples	Refinement parameters			Lattice parameters						
	R_{exp}	R_p	GoF	a (Å)	b (Å)	c (Å)	V (Å^3)	Orthorhombic distortion (b/a)	Exp. density, ρ (g/cm^3)	Average grain siz
BBNE0Y0	10.76	12.84	1.02	5.5439	5.5536	25.5975	788.111	1.00174	7.00919	1.39 ± 0.0278
BBNE4Y0	11.57	13.59	1.05	5.5441	5.5550	25.5976	788.341	1.00196	6.87240	1.42 ± 0.014
BBNE4Y2	10.39	14.93	1.46	5.5448	5.5551	25.5980	788.467	1.00185	6.83796	1.54 ± 0.0125
BBNE4Y4	10.13	13.53	1.35	5.5450	5.5552	25.5989	788.537	1.00183	6.72015	1.67 ± 0.1365
BBNE4Y6	10.01	14.46	1.44	5.5454	5.5561	25.5991	788.728	1.00192	6.77289	1.78 ± 0.0889
BBNE4Y8	7.07	8.64	1.07	5.5479	5.5601	25.6178	790.229	1.00219	6.47426	1.89 ± 0.1129
BBNE4Y10	7.27	9.19	1.08	5.5488	5.5612	25.6200	790.581	1.00223	6.76007	1.92 ± 0.1761
BBNE4Y12	10.21	14.87	1.45	5.5497	5.5600	25.6219	790.597	1.00185	6.01060	1.45 ± 0.0295

Table 1.1 Refinement and lattice parameters, experimental density, and grain size of all compositions of BBN

- Ankita and Renuka Bokolia reported that undoped, Er^{3+}-doped, and Er^{3+}/Yb^{3+} co-doped $BaBi_{2-x-y}Nb_2Er_xYb_yO_9$ ceramics show orthorhombic Fmmm symmetry with dense, square-like grains. FTIR confirmed Aurivillius peaks at 619 and 822 cm^{-1}, while Raman spectra increased from 4 modes (undoped) to 12 modes (doped). Nb–O bond lengths at 840 cm^{-1} were calculated using Herschbach's exponential relation.
- According to the authors, dielectric studies showed strong dispersion around Tm, frequency-dependent ε′ decrease, and diffused ε″ peaks, all confirming relaxor ferroelectric behaviour. Doping strengthened diffuseness and modified polar nanoregions.

- The authors highlighted thin P–E loops at 75–100 kV/cm and calculated W, Wrec, and η using Pm and Pr. Undoped, Er^{3+} doped, and Er^{3+}/Yb^{3+} co-doped BBN showed values of (0.683, 0.534, 78.25%), (0.471, 0.392, 83.39%), and (0.508, 0.461, 90.87%), respectively.
- They concluded that energy parameters were thermally stable (303–415 K) with only ~0.03% variation. While W and Wrec remained comparable, η increased with doping, and BBNE4Y4 showed the best ε′, diffuseness, and efficiency—suitable for advanced energy-storage applications.

1.3 LITERATURE REVIEW 2

Structural and ferroelectric modifications in SrBi2Nb2O9 Aurivillius phase compounds by Nd3+ion doping.[13]

-Zulhadjri*, Alfir Rizki, Tio Putra Wendari, Yulia Eka Putri

- Zulhadjri reported that Nd^{3+}-doped $SrBi_{2-x}Nd_xNb_2O_9$, synthesised via the molten salt method, retained a single-phase orthorhombic Aurivillius structure (A21am). Increasing Nd^{3+} reduced unit cell volume and orthorhombicity, confirming successful Bi-site substitution without disturbing the perovskite layer.
- all samples displayed the typical plate-like morphology of Aurivillius materials, while FTIR results confirmed the preservation of perovskite-layer bonding. The dielectric response exhibited a consistent. ferroelectric–paraelectric transition temperature (Tc), with higher Nd^{3+} levels promoting diffuse ferroelectric behaviour. These effects were attributed to the reduced influence of the Bi^{3+} $6s^2$ lone pair and lowered lattice distortion.Nd^{3+} levels promoting diffuse ferroelectric

behaviour. These effects were attributed to the reduced influence of the Bi^{3+} $6s^2$ lone pair and lowered lattice distortion.

- Zulhadjri highlighted that P–E loops remained non-saturated, especially at x = 0.275, indicating diffuse ferroelectricity. Nd^{3+} Incorporation effectively adjusted structural, dielectric, and ferroelectric properties, enhancing the material's potential for advanced ferroelectric applications.

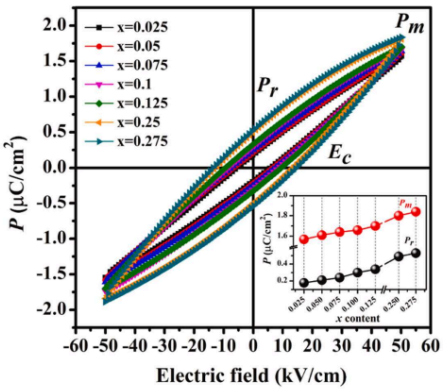

Fig 1.2: ferroelectric hysteresis loop (P–E) of SrBi2-xNdxNb2O9 measured at room temperature. The inset shows the polarisation (Pr and Pm) dependence on x content.

1.4 Research Objectives

- To synthesise single-phase Aurivillius-type $BaBi_2Nb_2O_9$ (BBN) ceramics doped with Nd^{3+}ions via solid state reaction method.
- Correlates microstructure and dielectric properties for different compositions of Nd^{3+}.
- To optimise the prepared compositions to attain maximum energy efficiency via the P-E hysteresis loop.
- Explore the possible applications in energy storage devices.

CHAPTER 2

METHODOLOGY

2.1 Materials and Reagents

Barium Carbonate [$BaCO_3$](99%), Bismuth(iii)oxide [Bi_2O_3](99.975%), Neodymium Oxide [Nd_2O_3](99.99%), Niobium(v)Oxide [Nb_2O_5](99.99%) was purchased from Sigma Aldrich.

2.2 Synthesis Methods

Solid state method

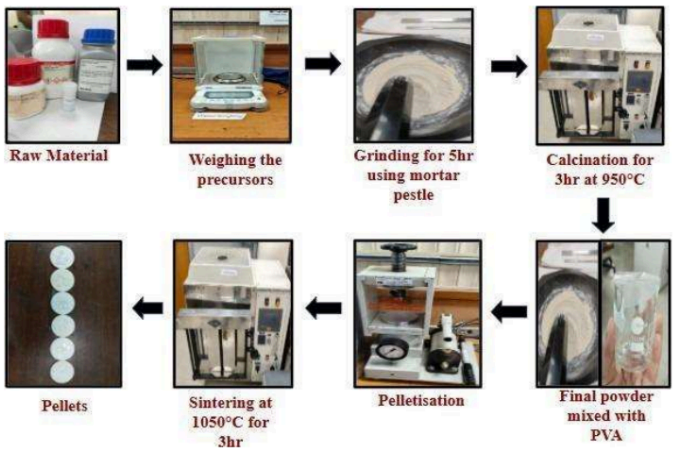

Fig. 2.1: Pictorial representation of synthesis of $BaBi_2Nb_2O_9$ (BBN) ceramics doped with Nd^{3+} ions.

The $BaBi_2Nb_2O_9$(BBN) and $BaBi_{2-X}Nb_2Nd_XO_9$ (x= 0.04,0.06,0.08, and 0.1) were synthesised by a conventional solid state method. Initially, the precursor powders were weighed stoichiometrically and ground thoroughly with a mortar and pestle for about 5 hrs by mixing ethanol(Sigma Aldrich) to maintain homogeneity of the sample. After

drying, the sample was then subjected to calcination at 950ºC for 3 hours in a closed alumina crucible. The calcined powders were then dry ground again to ensure uniformity. The Polyvinyl alcohol (PVA) was added to the final powder as a temporary binder (3-4 drops) and ground to a fine powder, then pressed into pellets of different sizes according to the characterisation using a hydraulic press. These pellets were sintered at 1050°C for 3 hours with a heating rate of 2°C per minute and 1 hour hold at 600°C for removing PVA in a high-temperature furnace to obtain the final $BaBi_{2X}Nb_2Nd_XO_9$ ceramics. After this, the obtained pellets will be polished on both sides using sandpaper to get a smooth and uniform surface for electrical characterisation. Then the density and porosity were measured using Archimedes' principle with distilled water as the medium. Apart from that, the resulting samples were characterised for their structural and optical properties.

2.3 Characterisation Techniques

The crystal Structure of the$BaBi_2Nb_2O_9$ and $BaBi_{2-X}Nb_2Nd_XO_9$ (x= 0.04,0.06,0.08, and 0.1) were studied using X-ray diffraction (XRD) with Cu Kα radiation of wavelength 1.5402 angstrom. Surface morphology was studied using a scanning electron microscope (SEM), and we have done the imaging using secondary electron 1 (SE1) to provide the possible highest resolution and detailed surface topographical data. The study reveals the average grain size and grain boundary of the crystal. The densities of the ceramics were measured using Archimedes' method, and the porosities were estimated to analyse the densification process of the sintered materials.
DC electrical conductivity measurements were carried out using sintered pellet samples coated with silver paste on both sides to ensure good electrical contact during the measurement process.

Fourier transform infrared (FTIR) spectroscopy was utilised to characterise the vibration and bonding nature of the NbO_6 octahedral units. In this case, for FTIR measurement, the

powder form of the samples prepared from the BBNB0 and BBNB4 compositions was selected. FTIR studies also facilitated the evaluation of local structural changes caused by Nd^{3+} ions.

Raman spectroscopic experiments were conducted at room temperature to probe the short-range ordering, lattice distortions, and local structural symmetry of the Nd-added ceramics. Further, the Raman results were interpreted to understand changes in vibration frequencies and Nb-O bonding.

The optical behavior of the prepared samples was determined by UV-visible diffuse reflectance spectroscopy (DRS). The optical bandgap energy was determined using the Kubelka–Munk function and Tauc plot analysis method to determine the effect of Nd doping on the electronic behavior of the material.

The ferroelectric nature of the sample was determined using Polarization-Electric Field (P-E) hysteresis loop analysis with respect to varying applied electric fields. In the case of P-E loops, the sintered pellets were mechanically polished and made thin to about 0.2 mm in thickness. On one surface of the sintered pellets, a paste of silver powder mixed with toluene was spread uniformly, whereas at the other surface, the silver-paste mixture was spread in the form of an electrode dot.

Dielectric (DE) studies were performed at wide temperatures and frequencies by employing an LCR meter to understand the properties of dielectric constant, dielectric losses, and phase transition in the ceramics. In case of dielectric studies, pellets with thickness more than 0.7 mm were employed. The silver paste-toluene combination was applied to both faces of the pellet surface without going to the sides so that no edge conduction influence occurs. To analyse the relaxor behavior of the samples, modified Curie-Weiss law was also considered.

CHAPTER 3

RESULTS AND DISCUSSIONS

3.1 XRD

Optimization of Calcination Conditions

Calcination conditions for obtaining pure-phase $BaBi_2Nb_2O_9$ ceramics had been optimized in terms of several variables, including calcination temperature, time period required for heating, heating rate, and precursor compositions. First, the variation in calcination temperatures ranging between 850 °C and 950 °C at a heating rate of 5 °C per minute was performed for 3 hours. The XRD results obtained on the calcined powders are compared with the JCPDS card no. 00-012-0403[12], illustrated in Fig. 3.1(a).

All compositions exhibit the characteristic diffraction peaks of the Aurivillius layered perovskite structure . An improvement in peak sharpness and intensity is observed with increasing calcination temperature, indicating enhanced crystallinity. However, an additional impurity peak persists in all samples, suggesting incomplete phase formation.

From all the studied temperatures, 950°C was found to be the best calcination temperature since it gives a higher degree of crystallinity without exceeding the temperature where substantial evaporation of Bi_2O_3 begins to occur. The further optimization of calcination was performed at 950°C through changes in calcination time and heating rate. While the diffraction peaks were significantly sharpened, the impurity peak did not disappear. This suggests that the formation of impurities does not depend much on the heating rate, but instead on the Bi deficiency resulting from Bi_2O_3 evaporation at high calcination temperatures.

The deficiency of Bi was addressed by adding 2 wt.% of excess Bi_2O_3 into the precursor formula, according to the literature reports that 2 wt.% is sufficient to yield phase-pure Aurivillius materials [13]. A smaller quantity of excess Bi_2O_3 may not suffice to cover the volatilization loss, while a larger quantity could cause segregation of Bi_2O_3 at grain boundaries, which would be harmful to the material's characteristics [13].

The XRD profile of the material obtained after calcination at 950 °C for 5 hours with a heating rate of 2 °C/min and 2 wt.% excess of Bi_2O_3 is presented in Fig. 3.1(b). It can be clearly observed that the absence of any impurity peaks signifies the formation of the pure phase Aurivillius-layered perovskite structure.

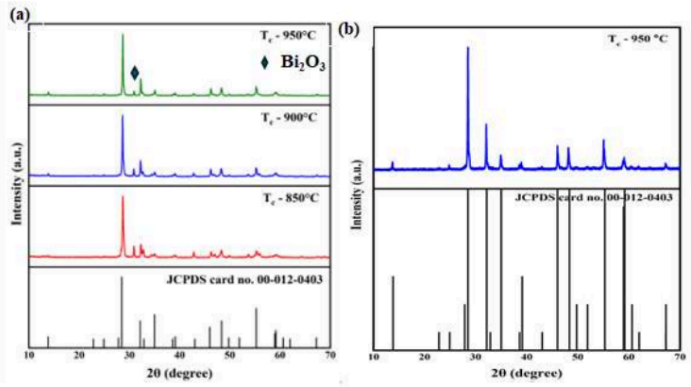

Fig.3.1 *XRD patterns of $BaBi_2Nb_2O_9$ ceramics showing* ***(a)*** *temperature optimization for calcination and* ***(b)*** *elimination of impurity phase upon addition of 2 wt% excess Bi_2O_3 at 950°C.*

Optimization of Sintering Conditions

The optimum sintering temperature for $BaBi_2Nb_2O_9$ ceramics was investigated by subjecting pure BBN green pellets to sintering processes conducted at 1000 °C, 1050 °C, and 1100 °C. Sintering was done using a uniform rate of heating of 2 °C/min for 3 hours. Before undergoing the actual sintering process, pure BBN green pellets underwent pre-sintering treatment at 600 °C for 1 hour to eliminate any trace of PVA binder that might still be present in the sample [14]. This procedure ensures that no residual organic matter will contaminate the ceramic body.

Figure 3.2 displays the X-ray diffraction pattern for the sintered pellets in comparison with the standard JCPDS card number 00-012-0403. The XRD patterns of all the samples consist mainly of typical diffraction peaks of the Aurivillius perovskite layered structure. But there are differences in the location of the peaks and phase purity with variations in sintering temperature.

The sintered pellet at 1000 °C shows the presence of the Aurivillius phase; however, the diffraction peaks show a small right shift, suggesting that there is some lattice shrinkage. This could be due to the partial loss of Bi^{3+} cations during the sintering process, creating an A-site vacancy [12,15].

On the other hand, the XRD pattern of the 1050 °C sintered sample reveals distinct peaks in good agreement with the standard JCPDS database. However, for the 1100 °C sintered sample, besides the main Aurivillius peaks, some impurity peaks also become observable, which could imply that secondary phases have formed due to excess Bi evaporation at higher temperatures.

According to the above XRD results, 1050°C can be considered as the best sintering temperature for BBN ceramics [15]. Consequently, using these optimal conditions, pure and Nd-doped BBN ceramics were prepared.

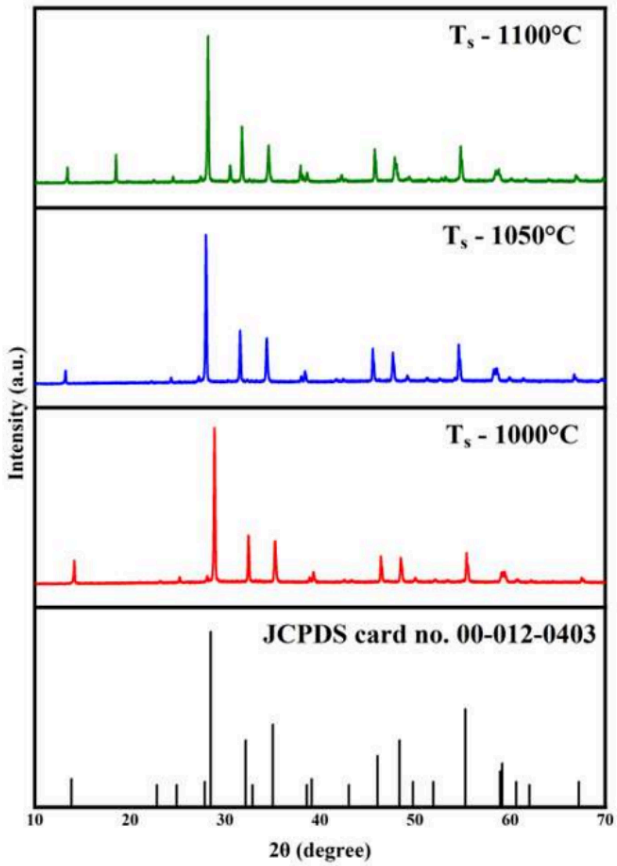

Fig.3.2 *XRD patterns of $BaBi_2Nb_2O_9$ ceramics sintered at 1000°C, 1050°C, and 1100°C, compared with the standard JCPDS card no. 00-012-0403, showing the effect of sintering temperature on phase purity.*

Phase Analysis of Pure and Nd doped BBN Ceramics

All the prepared samples exhibit a single-phase Aurivillius structure with no detectable impurity phases, and it matches the JCPDS data of the orthorhombic structure. In the Nd-

doped $BaBi_2Nb_2O_9$ system, the slight leftward shift of the XRD peaks indicates that Nd^{3+} ions influence the distortion caused by Bi^{3+} lone pairs, resulting in a small increase in lattice spacing and cell volume [3,9,10]. Changes in peak intensity further show that doping modifies the microstructure of the material. For all compositions, the strongest diffraction peak is observed at the (115) plane, confirming the typical Aurivillius phase associated with $BaBi_2Nb_2O_9$. Other major peaks include (002), (202), and (242). From the lattice parameter table, the b/a ratio of the BBNB4 sample comes out to be 1, which means the orthorhombic structure of the crystal is changing to a pseudo-tetragonal structure[5,12].

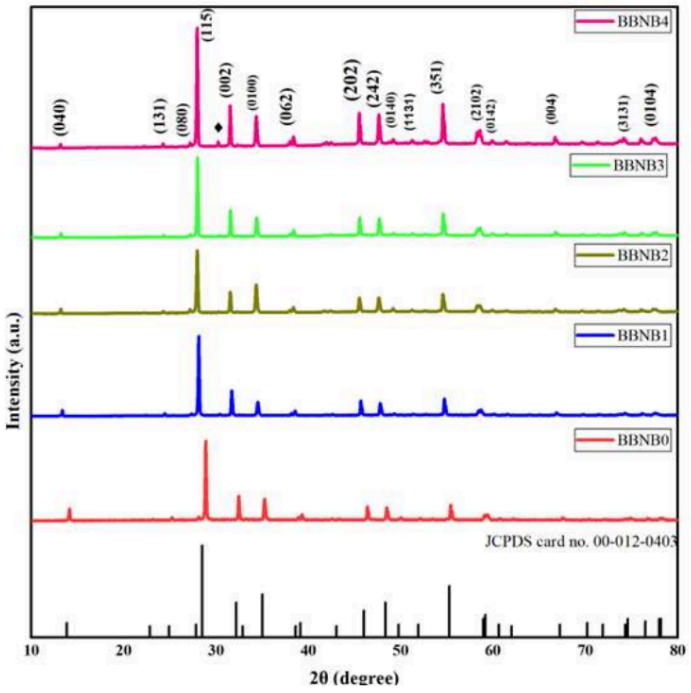

***Fig 3.3**. XRD plot of all compositions of BBN*

Sample	a (Å)	b (Å)	c (Å)	Volume (Å³)	b/a
BBNB0	5.5548	5.5611	25.5789	790.15	1.0011
BBNB1	5.5634	5.5696	25.5079	790.38	1.0012
BBNB2	5.5652	5.5714	25.5134	791.06	1.0011
BBNB3	5.5654	5.5709	25.5024	790.68	1.0009
BBNB4	5.5648	5.5624	25.5013	789.35	1.0004

Table 3.1. *lattice parameters of all compositions of BBN*

3.2 SEM

All the samples show tightly packed grains, which means the materials were well sintered and do not contain large pores. Nd doping leads to smaller grains, and the BBNB2 sample (x = 0.06) shows the most even and smooth grain structure. This good grain connection in the BBNB2 sample helps explain why its electrical properties are improved [18].

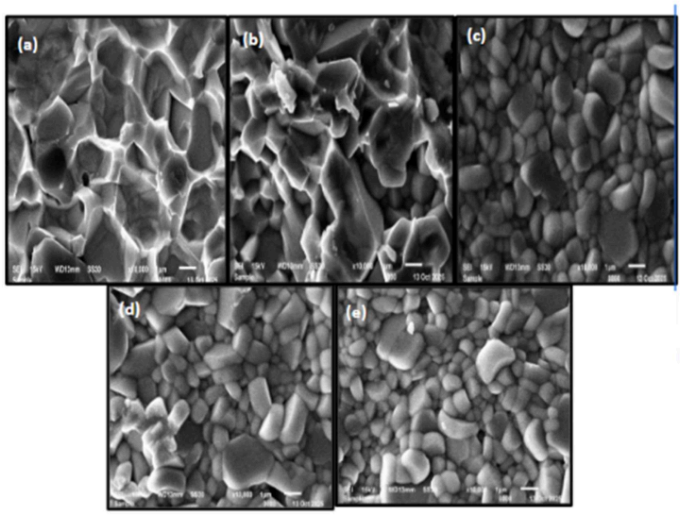

Fig 3.4: SEM micrograph of the all composition of BBN

3.3 Porosity and Density:

- **Porosity slightly increases with Nd doping**, leading to reduced density and minor microstructural looseness consistent with the reduced grain size seen in SEM images [11].
- Despite slightly higher porosity, the **BBNB2 (x = 0.06)** sample maintains good density (~7.13 g/cc) and shows the **best electrical performance**, indicating that its optimised grain structure compensates for porosity.

Formulae used: [20]

1. $\rho_{experimental} = m_{balance} / (m_{air} - m_{water})$ g/cc

2. $\rho\ (\%) = [(\rho_{theoretical} - \rho_{experimental})/\rho_{theoretical}]*100\%$

3. Theoretical value of density($\rho_{theoretical}$) = 7.52 g/cc

Fig 3.5: *Porosity measuring apparatus*

DC conductivity

This research paper focuses on investigating the electrical properties of $BaBi_2Nb_2O_9$ (BBN) ceramic material with Nd^{3+} ions concentration levels of x = 0, 0.04, 0.06, 0.08, and 0.10. The ceramic material samples were placed under a DC voltage of 20 volts for recording the electrical currents, from which resistivity, resistance, and conductivity were determined using the following formulae:

$$R=\rho \times t/A$$

$$\sigma=1/\rho$$

In the above equations, R denotes resistance, is resistivity, t represents the thickness, A indicates the area, and shows conductivity. Table displays the resistivity and conductivity values.

Composition	Average grain size (μm)	Density (ρ_{exp}) (g cm^{-3})	Porosity (p, %)	Resistivity (Ω cm)	Conductivity (Ω cm)$^{-1}$
BBNB0	1.79 ± 0.14	7.3297	2.53	7.80×10^{13}	1.28×10^{-14}
BBNB1	1.12 ± 0.03	7.2132	4.07	1.06×10^{14}	0.947×10^{-14}
BBNB2	1.07 ± 0.35	7.1327	5.15	3.50×10^{14}	0.286×10^{-14}
BBNB3	0.98 ± 0.03	7.1411	5.03	1.73×10^{14}	0.579×10^{-14}
BBNB4	0.99 ± 0.05	7.1886	4.41	1.70×10^{14}	0.588×10^{-14}

Table 3.2. *Average grain size, density, porosity, resistivity, and conductivity of undoped and Nd-doped BBN ceramics*

As seen from the analysis of the results, the DC conductivity of $BaBi_2Nb_2O_9$ ceramics doped with Nd^{3+} ions becomes lower with higher concentrations of dopants because of the increase in the resistivity values. It is associated with the changes detected in the microstructure of the samples based on the SEM images. Due to the incorporation of Nd^{3+} ions, the average grain sizes become lower; hence, more grain boundaries emerge inside the material. Grain boundaries are the sources of resistance that limit the movement of charge carriers, hence reducing DC conductivity [22]. Consequently, it was found that sample BBNB2 has the optimum grain boundary.

Analysis of Fourier transform infrared (FTIR)

The FTIR spectra recorded for the undated BBNB0 and doped BBNB1 samples reveal distinct absorption bands appearing near 566 cm^{-1}, 618 cm^{-1} and 822 cm^{-1}. These absorption bands are mainly associated with the characteristic banding and stretching vibrational modes of Nb—O bonds present in the NbO_6 octahedral units of the crystal structure [4,7,21]. The observed vibrational features confirm the formation of the niobate framework and indicate that the octahedral arrangement remains intact in both

compositions. Similar vibrational characteristics have also been reported for layered niobate and aurivillius type oxide ceramics [7].the corresponding spectra are presented in fig.3.6

After the incorporation of Nd^{3+} ions into the host lattice, a slight but noticeable shift in the bending vibrational band is observed. In the pure BBNB0 sample, the bending vibration appears around 618 cm^{-1} whereas in the Nd doped BBNB1 composition the peak shifts towards a higher wavenumber near 624 cm^{-1} as illustrated in fig. 3.7 and fig.3.8 . Such a shift toward higher frequency generally indicates a modification in the local bonding environment surrounding the NbO_6 octahedral [9]. This behaviour suggests that the Nd^{3+} ions are successfully incorporated into the lattice and influence the bond characteristics within the structure. Similar peak shift behaviour due to rare earth ion substitution has also been observed in Nd doped layered ferroelectric systems [6,22].

The shift in vibrational frequency may be attributed to variations in the Nb—O bond strength caused by the substitution of Nd ions in the crystal lattice. The presence of rare earth ions can alter the local atomic arrangement and produce slight changes in bond length and bond energy which consequently affect the vibrational behaviour of the Nb—O bonds. The increase in wavenumber indicates a possible strengthening of the bond interaction or local lattice distortion induced by Nd incorporation. Such modifications in the local structural symmetry are commonly associated with ionic radius mismatch and lattice strain generated during substitutional doping .

Furthermore, the full width half maximum values of the major absorption bands remain nearly unchanged for both BBNB0 and BBNB1 compositions as listed in Table . The absence of significant peak broadening indicates that Nd doping does not introduce considerable lattice disorder or the structural instability into the material. This observation suggests that the overall structural integrity of the NbO_6 octahedral framework is well

preserved even after rare earth ion incorporation. The retention of comparatively sharp absorption bands also reflects good crystallinity and structural ordering within the ceramic matrix.

The FTIR results therefore confirm that Nd doping modifies the local bonding environment without causing major disruption to the crystal structure. The retention of characteristic absorption bands together with minimal variation in FWHM demonstrates that the structural framework of the material remains stable after Nd incorporation. These findings are in good agreement with the XRD analysis which also confirms phase stability and preservation of the layered aurivillius structure in the Nd doped compositions.

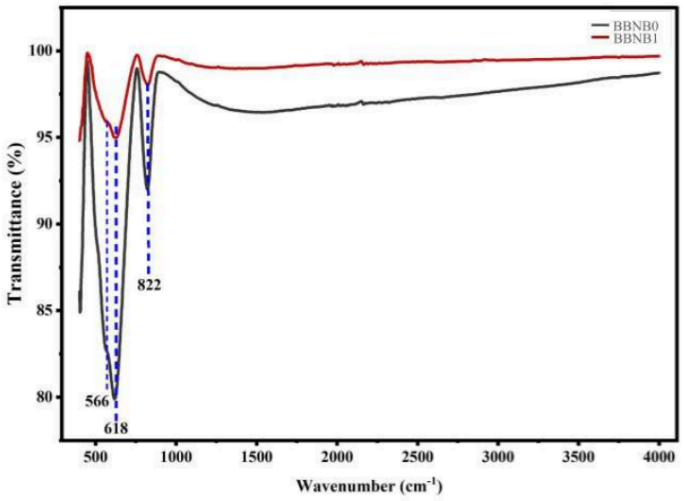

Fig. 3.6 *shows Fourier transform infrared (FTIR) data obtained at room temperature for BBNB0 and BBNB1 with prominent absorption peaks marked on 566 cm^{-1}, 618 cm^{-1} and 822 cm^{-1}.*

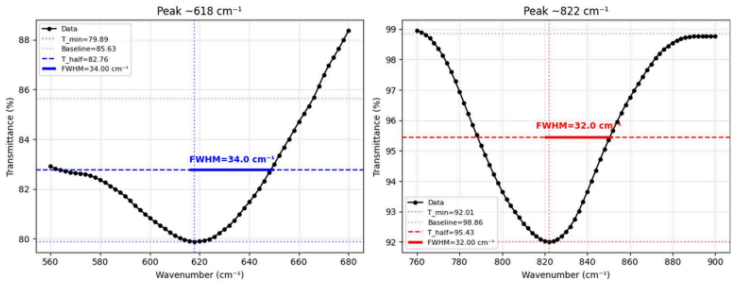

Fig.3.7 *FWHM analysis of FTIR absorption bands of BBNB0 at 618 cm^{-1} and 822 cm^{-1} using Direct method.*

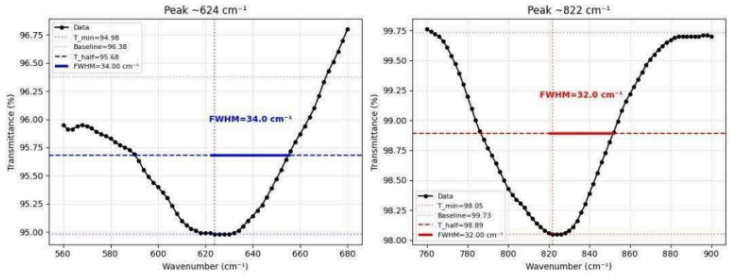

Fig. 3.8 *FWHM analysis of FTIR absorption bands of BBNB1 at 624 cm^{-1} and 822 cm^{-1} using Direct method.*

Sample	Vibrational Mode	Wavenumber (cm^{-1})	FWHM (cm^{-1})
BBNB0	Nb–O bending	618.00	34.00
BBNB0	Nb–O stretching	822.00	32.00
BBNB1	Nb–O bending	624.00	34.00
BBNB1	Nb–O stretching	822.00	32.00

Table 3.3. *Vibrational modes, corresponding wavenumbers, and FWHM values of FTIR absorption bands for BBNB0 and BBNB1.*

Raman Spectroscopy

Raman spectroscopy was employed to investigate the local structural modifications induced by Nd^{3+} substitution in $BaBi_2Nb_2O_9$ ceramics. Raman analysis is highly sensitive to short-range structural ordering and local lattice distortion, making it an effective technique for studying Aurivillius layered compounds. The room-temperature Raman spectra of all compositions (BBNB0–BBNB4), recorded in the range of 100–1200 cm^{-1} using a 660 nm excitation laser, are shown in Fig. 3.9.

All compositions possess almost identical characteristic Raman bands, implying that the introduction of Nd does not modify the long-range Aurivillius-layered crystal structure. This is in agreement with the X-ray diffraction findings and earlier work on BBN-based materials [26].

The Raman modes below ~250 cm^{-1} are mainly associated with Bi–O vibrations and translational lattice modes involving A-site cations [22,23]. The intermediate bands between 300–600 cm^{-1} correspond to bending and deformation vibrations of NbO_6 octahedra [23,24,26]. An intense band existing around 865 cm^{-1} is related to the stretching vibration of Nb-O bond with high sensitivity to octahedral distortion [23,25,28].

A weak band around ~198 cm^{-1} shows significant enhancement after Nd doping, implying that there are more localized distortions because of Bi site substitution [29]. Systematic composition-dependent changes in Raman peak positions and peak broadening are also observed with increasing Nd concentration.

From the figure (Fig. 3.10), it is clear that the symmetric stretching vibration of Nb-O (v9) undergoes red shift from 865.92 cm^{-1} to 862.17 cm^{-1} as the amount of substitution changes from BBNB0 to BBNB4. The Raman mode centered at ~304 cm^{-1} (v5) shows a slight blue shift, while a small red shift can be seen in the Raman peak centered at ~567 cm^{-1} (v8). These inconsistent mode-specific shifts imply that there is distortion of the NbO_6 octahedra without lattice expansion [24,27].

In addition, some Raman modes exhibit increased FWHM values due to the addition of Nd, which implies a higher degree of strain and disorder in the lattice structure.

Further analysis of the Nb-O stretching mode was performed by the application of Herschbach's equation:

$$\nu = A\, e^{BR}$$

where ν is the Raman frequency, R is the bond length, and A and B are empirical constants [9,24].

The calculated Nb–O bond length increases gradually from 1.773 Å for BBNB0 to 1.776 Å for BBNB4, confirming progressive elongation of Nb–O bonds with increasing Nd concentration. The local octahedral distortion and increased structural disorder disrupt long-range dipolar ordering and promote relaxor ferroelectric behaviour in Nd-modified BBN ceramics.

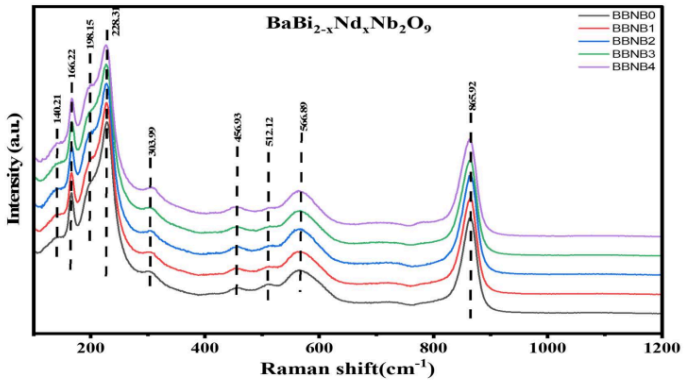

***Fig. 3.9**: Stacked Raman spectra of BBNB0–BBNB4 samples recorded at room temperature using a 660 nm excitation laser.*

Sample	Raman peak ν (cm^{-1})	Nb–O bond length R (Å)
BBNB0	865.9	1.7733
BBNB1	864.2	1.7744
BBNB2	864.1	1.7744
BBNB3	862.8	1.7752
BBNB4	862.2	1.7756

***Table 3.4**. Nb–O bond length estimated from Raman stretching mode using Herschbach's empirical relation.*

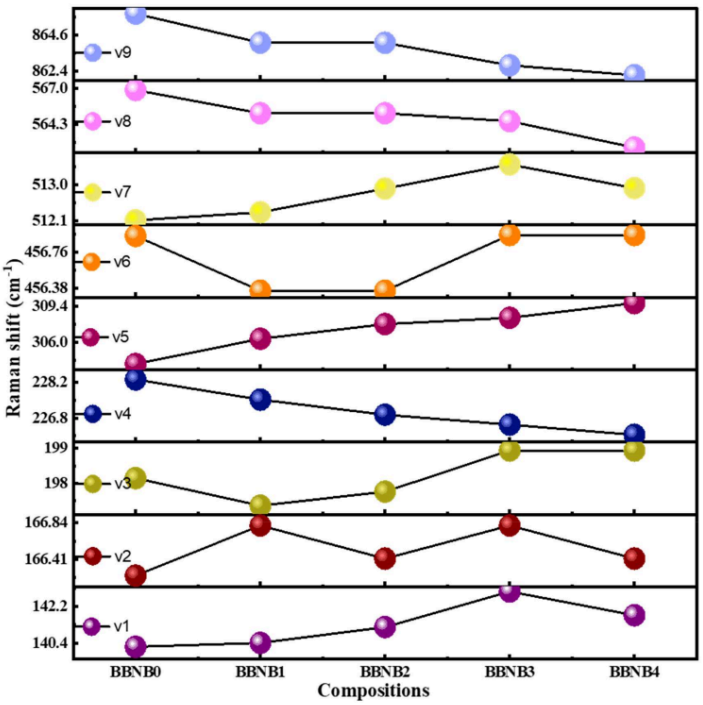

***Fig. 3.10**: Evolution of Raman peak positions (v1–v9) as a function of composition, illustrating composition-dependent peak shifts.*

Raman shift (cm^{-1})	Band assignment	Mode assignment	Structural origin	Reference

140.21	v1	Lattice vibrational mode	A-site (Ba/Bi)-O vibrations	[23, 24, 26]
166.22	v2	Bi-O related vibration	BiO_6 polyhedral dynamics	[23, 24, 26]
198.15	v3	Disorder-activated mode	A-site vibration/symmetry breaking	[23, 24, 26]
228.31	v4	Bi-O / octahedral tilting mode	Coupled A-site–octahedral vibration	[23, 24, 26]
303.99	v5	NbO_6 bending mode	Nb-O-Nb bending vibration	[24, 25]
456.93	v6	NbO_6 deformation mode	Octahedral distortion vibration	[24, 25]
512.12	v7	NbO_6 asymmetric bending	NbO_6 octahedral vibration	[24, 25]
566.89	v8	NbO_6 stretching-related mode	Nb-O vibration	[24, 25]
865.92	v9	Nb-O symmetric stretching mode	NbO_6 octahedral stretching	[25]

Table 3.5*. Raman mode assignments of the BBNB0 sample showing peak position, vibrational origin, and corresponding bonding units.*

Diffuse Reflectance Spectroscopy and Band Gap Analysis

The optical properties of Nd^{3+} doped barium bismuth niobate ceramics, $BaBi_{2-x}Nd_xNb_2O_9$ (x= 0.00, 0.04, 0.06, 0.08 and 0.10) were investigated using UV visible diffuse reflectance spectroscopy (DRS) in order to understand the influence of Nd incorporation on the electronic structure of the material. The diffuse reflectance spectra for all synthesized compositions are presented in Figure. . The spectra exhibit a distinct absorption edge within the visible region which is a typical characteristic of semiconducting oxide ceramics[30]. The presence of a sharp absorption edge indicates a good optical response and confirms the semiconducting nature of the prepared samples.

A gradual change in the position of the absorption edge is observed with increasing Nd^{3+} concentration. These variations suggest that the incorporation of Nd ions produces modifications in the electronic band structure of the $BaBi_2Nb_2O_9$ host lattice [23, 31]. The shift in optical absorption behaviour may arise due to changes in lattice parameters, local structural distortion and alteration in the interaction between metal and oxygen orbitals after rare earth ion substitution [30].

Rare earth doping is known to introduce localised electronic states in oxide ceramics without significantly disturbing the fundamental crystal framework of the material [29]. In the present system, Nd^{3+} ions are incorporated into the layered oxide structure while preserving the structural stability of the host material. The optical absorption process is mainly governed by electronic transitions between the valence and conduction bands of the host lattice. In addition weak absorption features associated with intra configuration 4f- 4f electronic transitions of Nd^{3+} ions may also contribute to the spectra. However, these transitions generally appear weak because the 4f electrons are effectively shielded by the outer 5s and 5p orbits minimising their interaction with the surrounding crystal field [32-34].

To estimate the optical band gap energy of the prepared ceramics, the diffuse reflectance data were analysed using the kulbeka- Munk theory which is commonly employed for optically thick polycrystalline samples [35]. The Kubelka- Munk function as:

$$F(R)=\frac{(1-R)^2}{2R}\frac{S}{\alpha}$$

Where R represents the diffuse reflectance and F(R) corresponds to the absorption function. In this relation the scattering coefficient is assumed to remain nearly constant over the measured wavelength range [35]. This method enables reliable conversion of reflectance data into absorption related information suitable for band gap analysis.

The optical band energy (Eg) was determined using the Tauc relation [36]:

$$[F(R)h\nu] = C(h\nu - Eg)^n$$

Where hν denoted the incident photon energy, C is a proportionality constant and n depends on the nature of the electronic transition involved. For the present layered oxide ceramic system, an incident allowed transition was assumed and therefore the value of n= 1/2 was considered during the analysis [36]. The photon energy was calculated using the relation:

$$h\nu = \frac{1240}{\lambda} \quad \text{(eV)}$$

Where hν is expressed in electron volts (eV) and λ represents the wavelength in nanometres.

The Tauc plots obtained from the variation of $[F(R)\ h\nu]^{1/2}$ with photon energy for different compositions are shown in Fig. 3.11.The linear portion of each curve was extrapolated towards the energy axis and the point of intersection was taken as the optical band gap value of the corresponding composition. The calculated band gap energies for all samples are summarized in table

The variation of optical band gap with Nd^{3+} concentration does not follow a linear trend. An initial increase in band gap energy is observed for lower Nd doping concentrations which may be attributed to local lattice distortion and internal strain produced by the substitution of Nd^{3+} ions at Bi^{3+} lattice sites. Such structural modifications can alter the Nb—O—Nb bond angles and reduce orbital overlap between neighboring atoms, thereby affecting the electronic band structure of the material [31, 37, 38].

At higher Nd concentrations partial relaxation of lattice strain may occur through the generation of oxygen vacancies and defect states within the crystal lattice. These defects introduce localized energy levels near the conduction or valence band edges leading to band tailing effects and a reduction in the effective optical band gap energy. Similar behaviour has been reported in several rare earth doped layered perovskite oxide systems where defect induced states strongly influence optical absorption characteristics [35].

Overall the DRS analysis clearly demonstrates that Nd^{3+} incorporation significantly influences the optical behaviour of $BaBi_2Nb_2O_9$ ceramics. The observed changes in absorption edge position and band energy are mainly associated with lattice distortion, defect generation and modification of the electronic structure induced by rare earth doping. These results confirm that Nd substitution can effectively tune the optical properties of BBN ceramics without causing major structural instability [31, 37, 38].

Sample code	Optical band gap E_g (eV)
BBNB0	2.6526
BBNB1	2.8424
BBNB2	2.7348
BBNB3	2.7069
BBNB4	2.6359

Table 3.6*. Optical band gap (E_g) measurements for BBNN0–BBNN4 samples were determined from UV–Vis diffuse reflectance spectra by applying the Tauc method.*

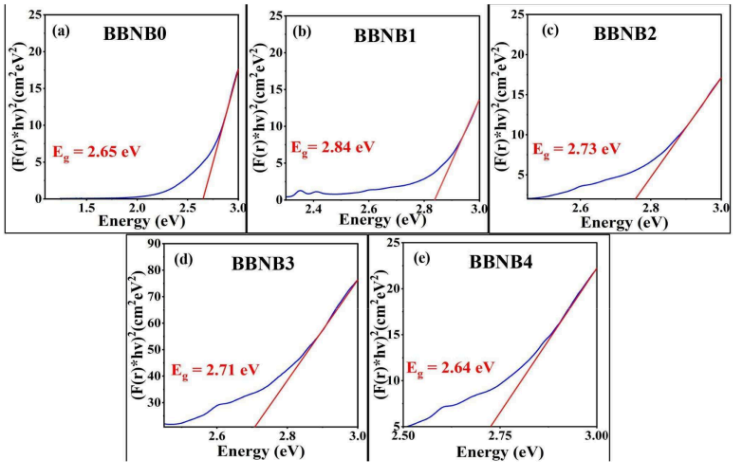

Fig. 3.11*.a-e Tauc plots of doped and undoped samples of BBN*

3.4 PE

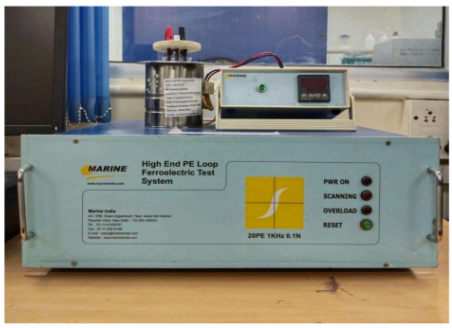

Fig 3.12. *P-E loop instrument*

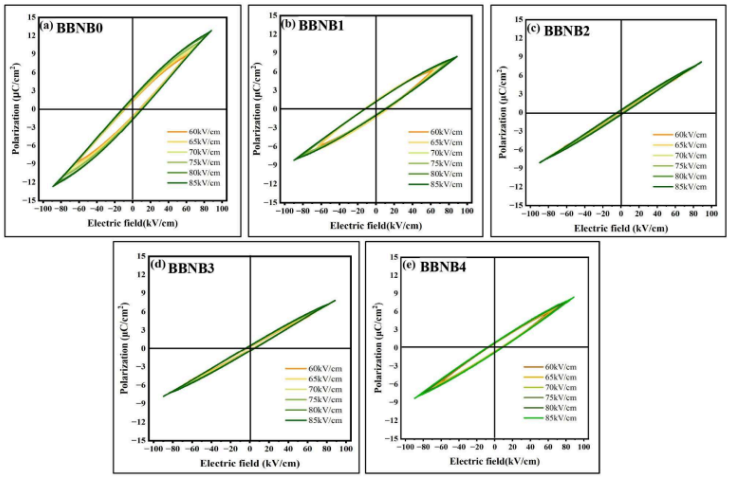

Fig 3.13. *PE loop of BBN for all compositions*

All the samples display slim P–E loops, which is a typical sign of relaxor-type ferroelectric behaviour with low hysteresis loss. The polarisation increases steadily with the applied electric field, showing that all compositions have a good dielectric response.

Among them, the BBNB2 sample (x = 0.06) shows a slightly wider loop, indicating better ferroelectric activity compared to the other doped samples. Nd doping also affects the domain-switching process and helps reduce leakage, which contributes to the improved functional performance of the material.

The temperature dependent PE loops of BBNN2 measured at 80 kV/cm exhibit slim hysteresis behaviour with only minor variations in the loop shape over the temperature range of 30-140 degree celsius, as shown in fig.3.15 (a) and (b), indicating excellent thermal stability and relaxor ferroelectric characteristics. The low remnant polarization and narrow hysteresis area contribute to enhanced energy storage efficiency and reduced energy loss. Furthermore, the nearly stable values of recoverable energy density (W_{rec}) and efficiency (η) with increasing temperature confirm the suitability of ceramic for high temperature energy storage application [9, 39-41].

The fatigue behaviour of the samples were examined up to 10,000 electric field cycles. The nearly invariant values of remnant polarization (P_r), maximum polarization (P_m), coercive field (E_c) and leakage current shown in fig.3.15 (c) and (d) indicate excellent fatigue endurance and stable ferroelectric switching characteristics .The absence of significant degradation confirms low defect accumulation and reduced domain wall pinning during repeated polarization reversal which demonstrates good electrical reliability of BBNN2 sample [13, 43].

Electric field (kV/cm)	**Parameter**	**BBNN0**	**BBNN1**	**BBNN2**	**BBNN3**	**BBNN4**
60	Pr ($\mu C/cm^2$)	1.2843	1.23239	0.21958	0.30193	0.73105
	Pm ($\mu C/cm^2$)	8.9383	6.29202	5.61874	5.34849	6.04715
	W (J/cm^3)	0.30808	0.23008	0.17766	0.17209	0.21181
	Wrec (J/cm^3)	0.21472	0.14414	0.16594	0.15145	0.15689

	η (%)	69.7	62.64	93.4	88.01	74.07
65	Pr (μC/cm²)	1.39823	1.39172	0.2325	0.35585	0.72396
	Pm (μC/cm²)	9.73321	6.87407	6.13541	5.08969	6.5156
	W (J/cm³)	0.35997	0.27285	0.20965	0.2035	0.24612
	Wrec (J/cm³)	0.25148	0.16751	0.19395	0.18244	0.18481
	η (%)	69.86	61.39	92.51	89.65	75.1
70	Pr (μC/cm²)	1.56329	1.23564	0.28094	0.39898	0.79493
	Pm (μC/cm²)	10.5574	7.54067	6.65207	6.41244	6.99468
	W (J/cm³)	0.41662	0.33048	0.24468	0.23894	0.27932
	Wrec (J/cm³)	0.29344	0.22785	0.22617	0.21226	0.21492
	η (%)	70.43	68.94	92.43	88.98	76.94
75	Pr (μC/cm²)	1.63576	1.16411	0.29708	0.39539	0.86946
	Pm (μC/cm²)	11.27434	7.5927	7.12999	6.8893	7.48442
	W (J/cm³)	0.48579	0.33465	0.28232	0.2798	0.32282
	Wrec (J/cm³)	0.33589	0.2318	0.25835	0.24341	0.24511
	η (%)	70.15	69.27	91.51	86.99	75.93
80	Pr (μC/cm²)	1.84282	1.17061	0.34875	0.43852	0.83752

	Pm ($\mu C/cm^2$)	12.16469	8.02192	7.63374	7.32542	7.90318
	W (J/cm^3)	0.54288	0.37647	0.32107	0.31455	0.35898
	Wrec (J/cm^3)	0.38115	0.26112	0.29395	0.27478	0.28246
	η (%)	70.2	69.36	91.55	87.36	78.68
85	Pr ($\mu C/cm^2$)	1.84282	1.23564	0.44562	0.49603	0.90849
	Pm ($\mu C/cm^2$)	12.85574	8.4674	8.18915	7.83223	8.47099
	W (J/cm^3)	0.60576	0.41892	0.37112	0.36059	0.41333
	Wrec (J/cm^3)	0.42964	0.29536	0.32914	0.30957	0.31732
	η (%)	70.92	70.5	88.69	85.85	76.77

Table 3.7. *PE parameters of all compositions of BBN*

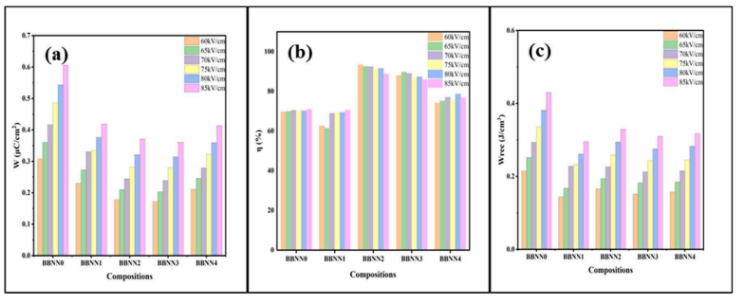

Fig. 3.14. a-e *Comparison bar graphs of total energy (W), efficiency (η), and energy recovered (w_{rec}) of doped and undoped samples of BBN*

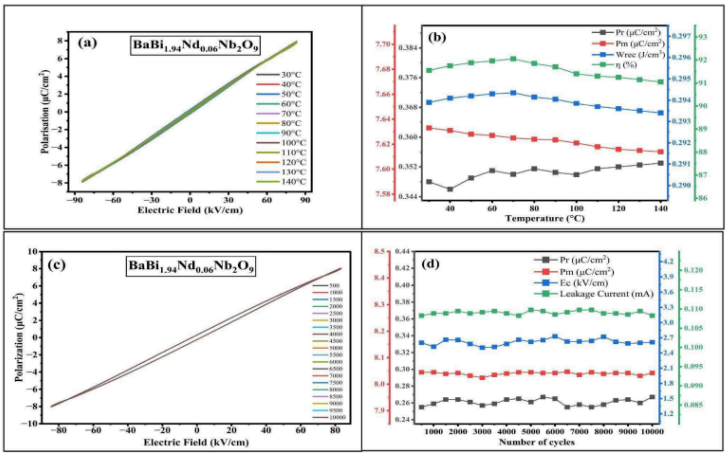

Fig. 3.15. (a) *Temperature-dependent polarization-electric field (P-E) hysteresis loops of* $BaBi_{1.94}Nd_{0.06}Nb_2O_9$ *ceramic recorded at an electric field of 80 kV/cm across temperature range from 30°C to 140°C.* ***(b)*** *Temperature dependence of the remnant polarization* (P_r)*, maximum polarization* (P_m)*, recoverable energy* (W_{rec}) *and energy efficiency* (η)*.* ***(c)*** *Fatigue behavior of the P–E loops measured from 500 to 10,000 switching cycles at 80 kV/cm.* ***(d)*** *Dependence of remnant polarization* (P_r)*, maximum polarization* (P_m)*, coercive field* (E_c) *and leakage current*(I_{leak}) *on the number of cycles.*

3.5 Dielectric Studies

The dielectric constant and the dielectric loss for different BBN compositions are shown in Fig. 3.17 and Fig. 3.18. These figures show the results for a range of frequencies from 1 kHz to 1 MHz. The BBN compositions have a dielectric maximum instead of a sharp peak. This means that the BBN compositions have a diffuse phase transition. This is typical of ferroelectrics [47, 48].

To understand the degree of diffuseness the dielectric data were analyzed using a law. This law is called the modified Curie-Weiss law [1, 49]. The law is expressed as:

$$\frac{1}{\varepsilon'} - \frac{1}{\varepsilon'_m} = \frac{(T - T_m)^\gamma}{C}$$

In this law ε′m is the peak constant at the temperature Tm. C is the Curie- constant. γ is the diffuseness parameter. For ferroelectrics γ is close to 1. For relaxor behavior γ values are close to 2. If γ is between 1 and 2 it means that the material has relaxor characteristics [4].

Fig. 3.19 Shows a correlation between the graph of ln(1/ε′−1/ε′m) and ln(T−Tm) at a frequency of 500 kHz for all the BBN compositions. The slope γ values measured are 1.7038 for BBNB0, 1.5233 for BBNB1, 1.7511 for BBNB2, 1.5310 for BBNB3, and 1.5831 for BBNB4. All these values are greater than one. This means that the BBN compositions have a diffuse phase transition and relaxor traits [9].

The high γ values for BBNB0 and BBNB2 mean that they have relaxor characteristics. The lower γ value for BBNB3 means that it has diffuseness. This could be because BBNB3 has an uniform structure. The dielectric loss shows maxima over temperature and frequency. This is typical of polarization. The lack of loss anomalies means that long-range ferroelectric ordering is minimal.

As the concentration of Nd increases the dielectric loss decreases. The BBNB4 sample has the overall loss. The relaxor behavior of the BBN compositions is mainly due to the disorder caused by Nd substitution. This substitution disrupts range dipolar order and creates polar nano-regions [50].

Although BBNB0 and BBNB2 have γ values, their energy-storage efficiency is not the same. The γ parameter only describes the degree of diffuse transition under low electric fields. The energy storage behavior is dependent on polarization reversibility and hysteresis loss under electric fields. In the Nd modified compositions, local structural disorder and dynamic polar nano-regions suppress domain wall motion and reduce remnant polarization. This results in energy dissipation [51].

The increase in constant for Nd substituted compositions is due to the distinct polarization mechanisms governing low field dielectric response and high field ferroelectric behavior. Nd substitution induces structural disorder and enhances polar nano region dynamics. This increases polarizability under low electric fields. However the same local disorder disrupts range ferroelectric domain ordering and suppresses complete dipole alignment under high electric fields. This results in reduced polarization and lower energy dissipation. Such behavior is characteristic of relaxor systems and is advantageous for dielectric energy storage applications [52].

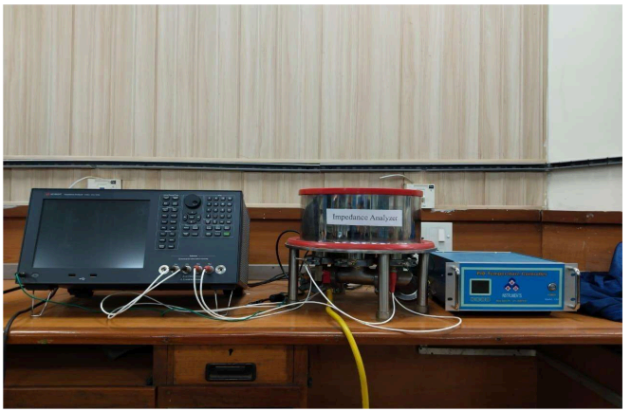

Fig 3.16. *DIELECTRIC INSTRUMENT*

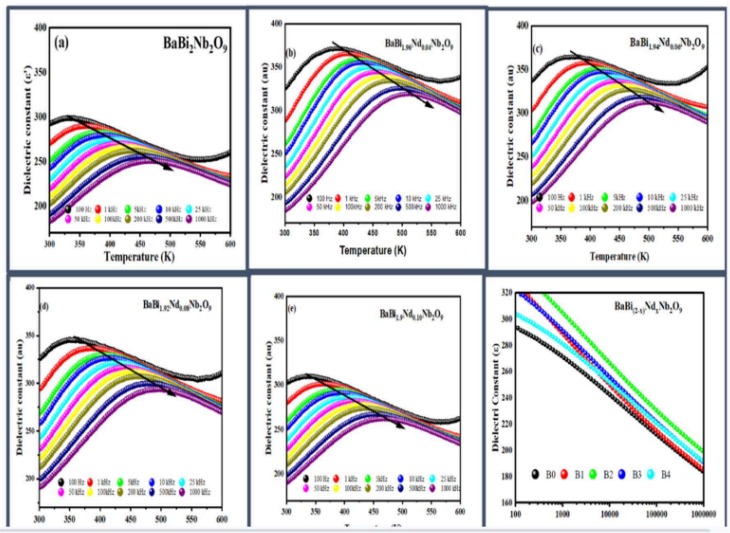

Fig 3.17. *(a,b,c,d,e) Dielectric constant vs temp graph and Dielectric const vs frequency (room temp) of* $BaBi_{2-X}Nd_XNb_2O_9$ *(x=0,0.04,0.06,0.08 and 0.1)*

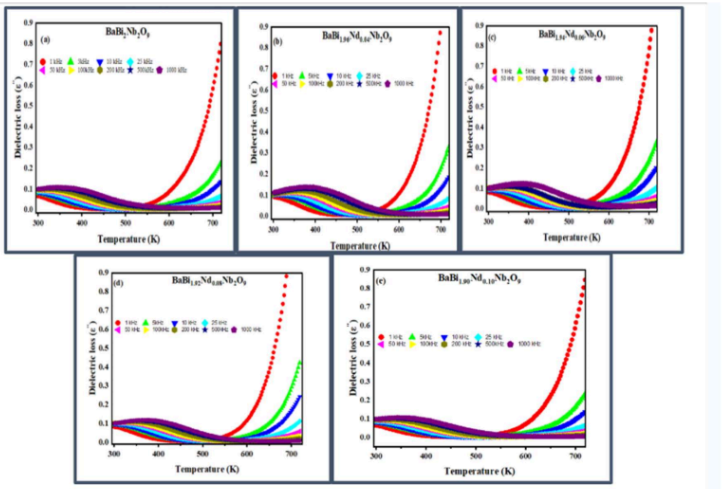

***Fig 3.18**. Dielectric loss vs temperature of all composition of BBN*

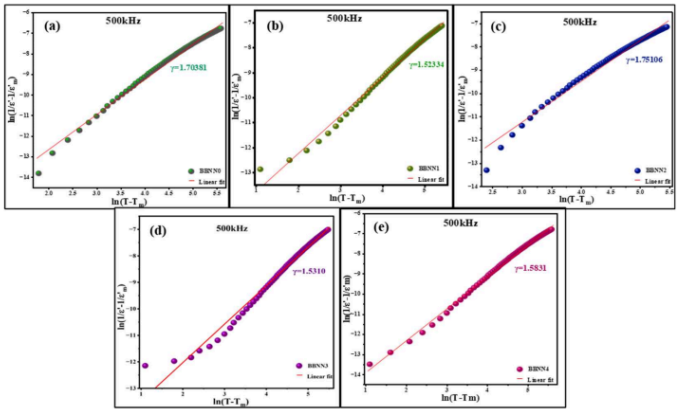

***Fig.3.19.** Modified Curie–Weiss analysis at 500 kHz for (a) BBNB0, (b) BBNB1, (c) BBNB2, (d) BBNB3, and (e) BBNB4 ceramics. The plots of ln(1/ε′ − 1/ε′$_m$) versus ln(T − T_m), along with linear fitting, are used to determine the diffuseness parameter (γ).*

CHAPTER 4

CONCLUSION

In the current study, Nd^{3+} doped $BaBi_2Nb_2O_9$ (BBN) Aurivillius ceramics with different compositions of $BaBi_{2-X}Nd_XNb_2O_9$ (x = 0.00, 0.04, 0.06, 0.08, and 0.10) have been successfully synthesized by employing the solid-state reaction method. The impact of Nd doping on the structural, microstructural, dielectric, ferroelectric and optical characteristics of BBN ceramics was systematically investigated. As per the outcomes, the incorporation of Nd leads to the effective manipulation of the electrical and structural properties of the material without altering the layered Aurivillius structure.

The XRD patterns revealed the existence of a single-phase orthorhombic Aurivillius structure in all the compositions without any formation of any other impurity phases under optimized synthesis conditions. The peak positions were found to be in accordance with the standard JCPDS card, confirming the single-phase nature of the ceramics. The minor shifting in the peak positions along with lattice parameters suggests the successful incorporation of Nd^{3+} ions into the Bi^{3+} site positions. The ratio of lattice parameters (b/a) is observed to approach 1 as the Nd content increases.

The SEM analyses indicated that there was an increase in the number of grains but with a finer grain size compared to that in the undoped one. Among all compositions tested, the BBNB2 composition (x = 0.06) had a denser microstructure and better grain connectivity, which led to higher electrical properties. The results obtained from density and porosity studies also corroborated this trend, whereby BBNB2 had a higher density of about 7.13 g/cc, although the porosity slightly increased due to the addition of Nd in the samples.

Both FTIR and Raman spectroscopic studies proved that the NbO_6 octahedral structure remained intact even after Nd doping. The FTIR absorption bands related to Nb–O

bending vibration frequencies were observed to have been modified from 618 cm^{-1} in the pure composition to 624 cm^{-1} in the Nd-doped composition. As for the Raman analysis, peaks were observed to depend on composition, showing slight shiftings and broadenings. In particular, the Nb–O symmetric stretching vibrations showed a shift from 865.92 cm^{-1} in BBNB0 to 862.17 cm^{-1} in BBNB4, and the Nb–O bond lengths calculated ranged from 1.7733 Å to 1.7756 Å, respectively.

The optical analysis done through diffuse reflectance spectroscopy indicated that the Nd substitution plays a role in determining the electronic structure and the optical absorption properties of the BBN ceramic materials. The optical bandgap was first raised from 2.6526 eV for BBNB0 to 2.8424 eV for BBNB1 and then lowered to 2.6359 eV for BBNB4. Such variations could be due to lattice strain, defects, and localized electronic states induced by the replacement of rare earth ions.

Ferroelectric analysis confirmed the presence of very small P-E hysteresis loops for all the compositions, which is consistent with relaxor ferroelectric behaviour with low hysteresis losses. Nd doping was able to lower the remnant polarization but improve energy storage efficiency. Out of all compositions, the highest energy efficiency of approximately 93.4% at 60 kV/cm was observed for BBNB2. For BBNB2, the efficiency remained above 91% under larger electric fields. With an electric field of 85 kV/cm, the recoverable energy density (W_{rec}) was found to be 0.32914 J/cm^3 for BBNB2 with low remnant polarization.

Dielectric studies revealed diffuse ferroelectric–paraelectric phase transitions in the temperature range of 400–450 K for all compositions. The dielectric constant exhibited strong frequency dependence, confirming relaxor ferroelectric characteristics. The diffuseness parameter (γ) obtained from the modified Curie–Weiss relation was found to be greater than 1 for all compositions, further supporting diffuse phase transition

behaviour. The highest γ value of 1.7511 was observed for BBNB2, indicating enhanced relaxor nature compared to other samples. In addition, BBNB2 consistently exhibited higher dielectric constant values together with lower dielectric loss, demonstrating improved dielectric stability and electrical response.

Overall, the present study establishes that Nd^{3+} substitution is an effective strategy for tuning the structural and functional properties of $BaBi_2Nb_2O_9$ ceramics. Among all investigated compositions, BBNB2 (x = 0.06) exhibited the most balanced combination of dielectric, ferroelectric, optical, and microstructural properties. The enhanced energy efficiency, stable dielectric behaviour, and preserved structural integrity make Nd-doped BBN ceramics promising candidates for applications in energy-storage devices, high-temperature capacitors, and advanced lead-free electronic components.

CHAPTER 5

FUTURE SCOPE

The results of this study show that Nd-doped BBN ceramics have strong potential for advanced dielectric and ferroelectric applications. In the future, additional efforts can be made to enhance their performance by investigating various doping concentrations or combining Nd with other rare earth elements to attain superior relaxor behaviour and energy storage potential. In depth investigations into grain boundary management, domain behaviour, and charge transport processes can aid in comprehending how to enhance the material for device requirements. Since the BBNB2 composition (x = 0.06) showed the best overall properties, it can be further tested under real operating conditions such as high temperature, high electric field, and long term cycling. These materials can also be evaluated for use in power electronic capacitors, temperature stable sensors, and energy storage systems. With more research and device level testing, Nd-doped BBN

ceramics could become reliable candidates for next generation high performance dielectric components.

Thesis_plag_report_1.docx

ORIGINALITY REPORT

8%	5%	6%	1%
SIMILARITY INDEX	INTERNET SOURCES	PUBLICATIONS	STUDENT PAPERS

PRIMARY SOURCES

1	www.science.gov Internet Source	2%
2	Ankita Banwal, Manoj Verma, Bharti Singh, Renuka Bokolia. "Temperature stability and improved energy storage efficiency of BaBi2Nb2O9: Er3+/Yb3+ relaxor ferroelectric ceramic under moderate electric fields", Applied Physics A, 2024 Publication	1%
3	link.springer.com Internet Source	1%
4	M. Naveed Ul-Haq, Tayyaba Yunus, Arif Mumtaz, V.V. Shvartsman, Doru C. Lupascu. "Magnetodielectric effect in relaxor/ferrimagnetic composites", Journal of Alloys and Compounds, 2015 Publication	<1%
5	Submitted to Indian Institute of Technology Guwahati Student Paper	<1%
6	archive.org Internet Source	<1%
7	ouci.dntb.gov.ua Internet Source	<1%
8	Zulhadjri, Alfir Rizki, Tio Putra Wendari, Yulia Eka Putri. "Structural and ferroelectric modifications in SrBi2Nb2O9 Aurivillius phase	<1%

compounds by Nd3+ ion doping", Materials Chemistry and Physics, 2024
Publication

9	Saloni Pendse, Jie Jiang, Yuwei Guo, Lifu Zhang et al. "Unit-Cell-Thick Oxide Synthesis by Film-Based Scavenging", The Journal of Physical Chemistry C, 2020 Publication	<1 %
10	ris.utwente.nl Internet Source	<1 %
11	Bandgar, A.B., S.R. Sabale, and S.H. Pawar. "Synthesis of nanocrystalline titanium dioxide using refluxed aqueous peroxy titanium complex solution", Micro & Nano Letters, 2011. Publication	<1 %
12	Submitted to Jawaharlal Nehru University (JNU) Student Paper	<1 %
13	Ullah, A.. "The effects of sintering temperatures on dielectric, ferroelectric and electric field-induced strain of lead-free Bi"0"."5(Na"0"."7"8K"0"."2"2)"0"."5TiO"3 piezoelectric ceramics synthesized by the sol-gel technique", Current Applied Physics, 201011 Publication	<1 %
14	H.R Rukmini, R.N.P Choudhary, V.V Rao. "Structural and electrical properties of sol–gel prepared (La,Li) modified PZT ceramics", Materials Letters, 1998 Publication	<1 %
15	Wen-Bo Li, Di Zhou, Ran Xu, Li-Xia Pang, Ian M. Reaney. " BaTiO –Bi(Li Ta)O , Lead-Free Ceramics, and Multilayers with High Energy	<1 %

Storage Density and Efficiency ", ACS Applied Energy Materials, 2018
Publication

16	Coondoo, I.. "Structural, dielectric and electrical studies in tungsten doped SrBi"2Ta"2O"9 ferroelectric ceramics", Ceramics International, 200701 Publication	<1 %
17	ijsrset.com Internet Source	<1 %
18	orbilu.uni.lu Internet Source	<1 %
19	Ankita Banwal, Bhavya Kumar, Manoj Verma, Ankur Shandilya, Bharti Singh, Renuka Bokolia. "Improved optical characteristics in BaBi2Nb2O9 ferroelectric ceramic infused with transition metal ion (W6+) and rare earth ions (Er3+/Yb3+)", Journal of Luminescence, 2024 Publication	<1 %
20	Megha Narwan, Ankita Banwal, Bhavya Kumar, Manoj Verma, Ankur Shandilya, Vineet Kumar Rai, Richa Sharma, Renuka Bokolia. "Ho3+- driven novel orange emission and enhanced energy storage in lead-free Bi0.5Na0.5TiO3 ceramics", Ceramics International, 2025 Publication	<1 %
21	Nazia Khatun, Sajib Ahmed, Mohammad Sajjad Hossain, Syed Farid Uddin Farhad et al. "Influence of Y3+ and La3+ ions on the structural, magnetic, electrical, and optical properties of cobalt ferrite nanoparticles", Heliyon, 2023 Publication	<1 %

22	sciendo.com Internet Source	<1 %
23	Fergy John, Jijimon K. Thomas, John Jacob, Sam Solomon. "Electrical and Optical Properties of Nanocrystalline A8ZnNb6O24 (A=Ba, Sr, Ca, Mg) Ceramics", Journal of Electronic Materials, 2017 Publication	<1 %
24	Nurul Pratiwi, Yulia Eka Putri, Tio Putra Wendari, Andon Insani, Zulhadjri. "Structure-property relationship in Sn2+-doped PbBi2Nb2O9: Toward tunable dielectric and optical characteristics", Materials Science in Semiconductor Processing, 2026 Publication	<1 %
25	S. Shanmuga Sundari, Binay Kumar, R. Dhanasekaran. "Synthesis, dielectric and relaxation behavior of lead free NBT–BT ceramics", Ceramics International, 2013 Publication	<1 %
26	Submitted to Universitas Andalas Student Paper	<1 %
27	Zulhadjri, Alfir Rizki, Muhammad Agung Andri, Tio Putra Wendari, Yulia Eka Putri, Upita Septiani, Rahmayeni, Imelda. "Structure-Property Correlation in La3+-Substituted SrBi2Nb2O9 Ferroelectric Ceramics Synthesized via Molten Salt Route", Materials Research, 2026 Publication	<1 %
28	arxiv.org Internet Source	<1 %
29	pdffox.com Internet Source	<1 %

30	scholarbank.nus.edu.sg Internet Source	<1%
31	studymoose.com Internet Source	<1%
32	waseda.repo.nii.ac.jp Internet Source	<1%
33	www.mdpi.com Internet Source	<1%

Exclude quotes	On	Exclude matches	< 8 words
Exclude bibliography	On		

Thesis_plag_report_1.docx

GRADEMARK REPORT

FINAL GRADE

/0

GENERAL COMMENTS

PAGE 1

PAGE 2

PAGE 3

PAGE 4

PAGE 5

PAGE 6

PAGE 7

PAGE 8

PAGE 9

PAGE 10

PAGE 11

PAGE 12

PAGE 13

PAGE 14

PAGE 15

PAGE 16

PAGE 17

PAGE 18

PAGE 19

PAGE 20

PAGE 21

PAGE 22

PAGE 23

PAGE 24

PAGE 25

PAGE 26

PAGE 27

PAGE 28

PAGE 29

PAGE 30

PAGE 31

PAGE 32

PAGE 33

PAGE 34

PAGE 35

PAGE 36

PAGE 37

PAGE 38

PAGE 39

PAGE 40

PAGE 41

PAGE 42

PAGE 43

PAGE 44